Wireless Power Transmission for lunar applications

Wireless Power Transmission for lunar applications.

Erica Scantamburlo
Department of Mechanical and Aerospace Engineering
Politecnico di Torino
Torino, Italy
erica.scantamburlo@polito.it
ORCID: 0000-0003-1556-1102

Marco Luigi Ottavi
Department of Mechanical and Aerospace Engineering
Politecnico di Torino
Torino, Italy
marco.ottavi@polito.it
ORCID: 0009-0003-1137-012X

Domenico Edoardo Sfasciamuro
Department of Mechanical and Aerospace Engineering
Politecnico di Torino
Torino, Italy
domenico.sfasciamuro@polito.it
ORCID: 0009-0006-9693-3105

Leonardo Pappalardo
Department of Mechanical and Aerospace Engineering
Politecnico di Torino
Torino, Italy
leonardo.pappalardo@polito.it

Ivano Verzola
Lazzero Tecnologie srl
Strada Baldissero ,78 - Chieri (TO)
ivano.verzola@lazzero.com

Stefano Mauro
Department of Mechanical and Aerospace Engineering
Politecnico di Torino
Torino, Italy
stefano.mauro@polito.it
ORCID: 0000-0001-8395-8297

***Abstract*— Wireless Power Transmission (WPT) is a viable technique to ensure continuous energy supply on the lunar surface, independent of lunar night cycles and location. A constellation of satellites orbiting the Moon, with the goal of collecting solar energy through their own solar panels and transmitting it to the surface via laser beam, allows for energy potentially anywhere on the lunar surface and surviving the lunar night in both energy and thermal terms. This paper analyzes the possible orbits of satellites to provide power for the most part of the lunar surface, starting with the lunar South Pole, which currently presents itself as the most interesting area for upcoming missions and future lunar bases. In addition, the requirements and possible solutions for the satellite navigation system around the Moon and the laser beam pointing system are discussed.**

Keywords*— *Wireless Power Transmission, Lunar Economy, Lunar Orbits, Lunar Navigation, Laser Pointing System

I. Introduction

The world's leading space agencies and private aerospace companies have been preparing for years now for the human return to the Moon. In fact, this return marks the beginning of a new era for sustained and strategic use of lunar resources. In particular, NASA's Artemis II mission, whose launch is scheduled for 2026, aims at determining the human presence beyond the Earth orbits Artemis II is part of the "Artemis" program, developed by NASA whose primary objective is the establishment of the human presence on the Moon. Artemis III is planned to land the astronauts on the south pole of the Moon.

One of the biggest challenges in this decade-long effort is to establish a reliable energy supply on the lunar surface. In fact, this represents a key factor for supporting the infrastructures that are essential for the aid of human life and operations.

A dense cluster of landing sites is concentrated in the lunar south pole: this location offers a unique combination of resources and conditions that make it ideal for long-term exploration for three main reasons: permanently shadowed craters that may hold abundant water ice, elevated ridges with continuous sunlight and a scientifically rich environment. This includes a wide variety of geological features with ancient rocks and minerals; the South Pole–Aitken Basin, one of the oldest and largest impact basins in the Solar System; potential presence of volatiles like ammonia, carbon dioxide, and organic compounds; unique solar and radiation interactions with the lunar surface; and extreme environmental conditions that serve as analogs for other planetary bodies.

In [1], NASA conducts a study of the future lunar power request, envisioning various mission scenarios over time and different available technologies. Initially, the power demand will be of the order of a few kilowatts for the first scientific explorations. This demand increases drastically during the initial phases of demonstrating human habitability, early ISRU activities, and more distant explorations, reaching hundreds of kilowatts. Finally, envisioning space manufacturing infrastructures and commercial operations after 2040, power demand is foreseen to reach the order of gigawatt. At these high levels of energy demand, it is clear that solutions that contemplate classic solar panels [2] are highly inefficient due to the Moon's unique morphology, which creates PSRs, and the long lunar night (up to 14 days). Therefore, several alternative solutions are being studied, starting with vertical solar panels [3] placed in specific areas almost perpetually exposed to the Sun at a certain height. Other technologies under development include nuclear microreactors [4] and Primary Fuel Cells.

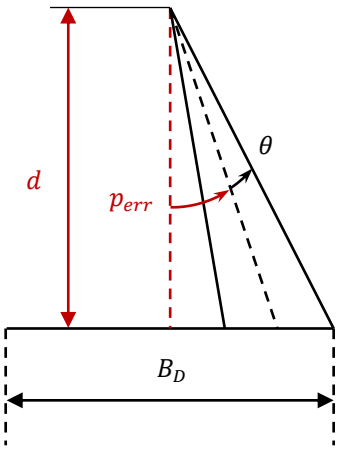

Figure 1: Laser Pointing Scheme.

Wireless Power Transmission (WPT) solution [5] fits into this scenario. A constellation of satellites orbiting the Moon could collect solar power and transmit it whenever the

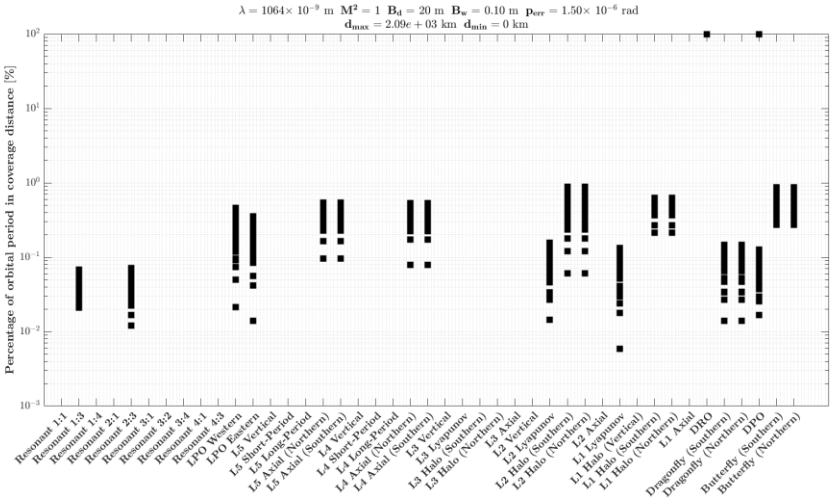

Figure 2: Percentage of orbital period spent in coverage distance from the Moon surface for all the sub-families of orbits in the CR3BP with range requirement d_{max}=1800 km.

satellite passes over a special receiver placed on the lunar surface. Transmission would be provided by laser radiation, which in the absence of the atmosphere would be loss-less in the path. This technology is explained in its various subsystems in [6] [7]: each satellite is equipped with a high-powered laser source, a precision pointing system based on several stages isolated from each other, and a thermal dissipation system to dissipate the heat leaving the laser source. The laser is a high-power fiber laser that has a typical total efficiency of around 30 percent [8].

WPT technology using laser technology is also extremely valuable for transmission on the lunar surface itself. In fact, imagining a living and working infrastructure distributed over distances of kilometers, in addition to the problem of energy production, there is also the problem of distribution.

II. LUNAR ORBIT SELECTION

A. *Laser Beam Pointing Scheme*

To perform a preliminary evaluation of orbits that are suitable for WPT, it is necessary to address beam divergence, together with size and shape of ground receivers. For this purpose, we use a simplified pointing scheme, represented in Figure 1. We notice that we assume that the ground receiver is spherical. Hence, the maximum admissible distance between the laser source and the ground receiver d_{MAX} is computed as follows:

$$d_{MAX} = \frac{B_D}{2\tan(p_{err} + \theta)} \tag{1}$$

where B_D is the diameter of the cross-section of the spherical ground receiver, p_{err} is the maximum pointing error (i.e. the 3σ pointing error) and θ is the beam half-width.

Furthermore, we notice that the value of p_{err} depends on the performance of the attitude and orbit determination & control System (AODCS) and of the laser pointing system. State-of-the-art space telescopes manage to reach a 1σ pointing precision in the order of $0.1''$. In our analysis, we suppose that the system can achieve a 3σ radial precision of $0.3''$. The value of θ depends instead on the parameters of the laser source and is computed as follows:

$$\theta = \frac{M^2 \lambda}{\pi B_W} \tag{2}$$

Where λ is the laser wavelength, M^2 is the beam-quality parameter ($M^2 \geq 1$) and B_W is the beam waist (i.e. minimum beam radius), that also determines the dimensions of the laser mirror.

WPT for Moon applications makes use of high-power lasers, in the order of tens of kW, for which Ytterbium Doped Fiber Lasers are particularly suitable. [6] The associated λ is 1064 nm, while M^2 depends on the technological performance. A somewhat reasonable guess is $M^2 = 1.2$ [9] . B_W can instead be chosen as a design parameter and, depending on mission requirements, its value increased to reduce beam divergence. The same is true for the size of ground

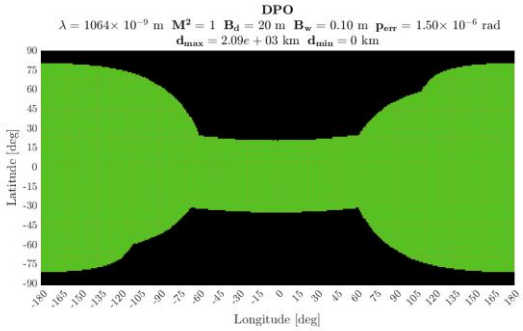

Figure 3: Surface Coverage Grid for DRO Orbits. Area in green is covered.

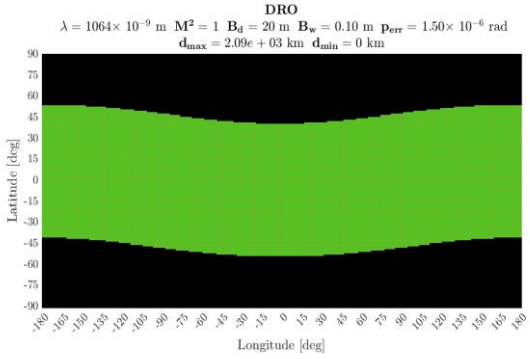

Figure 4: Surface Coverage Grid for DPO orbits. The area in green is covered.

receivers B_D, which can be varied to accommodate different mission scenarios.

B. Evaluation of Suitable Orbits

In [10], it is shown the case of Low Lunar Orbits (results are presented form altitude $h \leq 200\,km$). We highlight that there are four known inclinations (referring to the Moon Principal Axes Frame), at which circular orbits remain frozen (i.e. at least one of the mean orbital parameters is fixed). These inclinations are $\sim 27°, 50°, 76°$ and $86°$. In [11] the authors obtain two Walker constellations of quasi-frozen lunar orbits, at the altitudes of 260 km and 520 km, and with an inclination of 84°. The procedure is based on numerical methods.

We can then start by assuming a nominal reference orbit: a circular orbit at 600 km altitude, with an inclination of 85°. If we consider a minimum elevation angle of 30° for a line-of-sight link between the ground receiver and satellite (avoiding obstructions by Moon's terrain morphology), we can compute the range at which the satellite enters the transmission cone. If we impose that this is d_{MAX} and make use of Equation (1) and (2) with a ground receiver of 10 m in diameter, we obtain roughly $B_W \approx 10\,cm$. This magnitude is that of the mirror of a space telescope, and it is to be expected for the level of precision required. Further system-level trade-offs will lead to a more accurate guess but, for the sake of our study, we use this nominal orbit to make preliminary conclusions in the navigation and laser pointing departments. It is also interesting to compare the nominal case with orbits originating within the circular restricted three-body problem (CR3BP), for which we use the database provided by NASA JPL[1]. Since the Moon orbital and rotation periods are equal, it is sufficient to propagate these orbits for one orbit period in the synodic frame to obtain useful information on the ground coverage they provide. We also account for the effect of the North-South libration, caused by lunar obliquity. Nevertheless, we observe that this does not significatively modify the results and conclusions of this analysis. In addition, we choose $M^2 = 1$ and $B_D = 20\,m$, positioning ourselves in a more favorable case with respect to the nominal one.

The results reveal that not only the poles are well covered, but it is also possible to obtain global surface coverage using solely CR3BP orbits. However, as shown in Figure 2, only a small percentage (e.g. for this case less than 1%) of the total orbit period (which is in the order of tens of days) is spent at less than d_{MAX} from the Moon surface for the different sub-families. This is true even for larger values of d_{MAX}, to the point where engineering limitations come into play in limiting the associated B_D and B_W values. The sole exceptions are distant retrograde orbits (DROs) and distant prograde orbits (DPOs), for which we have trajectories providing coverage for 100% of their orbital period (the orbit period is in the order of 3-5 hours for these cases). Nevertheless, as shown in Figure 3 and Figure 4, they appear to be unsuitable to cover polar regions. For the remainder of this study, we will then focus on the previously mentioned nominal orbit.

III. Navigation System

Navigation in the lunar environment is still in its early stages and requires further development. To overcome the challenges related to communication delays, signal blockages and weak transmission, it is crucial to have an autonomous system capable of handling real time position and attitude determination. The absence of a stable magnetic field, the presence of solar wind, and lunar gravitation anomalies further complicate navigation. Current solutions involve the combination of optical sensors, such as star trackers and horizon sensors, with crater detection techniques to determine the satellite's position; current performance indicates an accuracy of about 100 meters which is insufficient to meet the accuracy requirements of advanced missions. The use of inter-satellite links could improve the accuracy of position determination, but filter stability remains a significant challenge, particularly in ensuring long-term continuity and reliability. For attitude determination, star trackers, sun sensors and gyroscopes are used. Algorithms such as MEKF (Multiplicative Extended Kalman Filter) are essential to achieve high pointing accuracy. However, current performance cannot always provide sufficient stability to cope with lunar environmental difficulties. Various sensor modalities have been proposed to enable autonomous navigation and localization in lunar orbit. For example, star trackers, while widely used for attitude determination, require unobstructed views of the star field and minimal stray light interference. Their performance is heavily dependent on precise alignment correction. Horizon-based navigation systems, which rely on identifying the lunar limb, are constrained by the need to orient cameras toward the horizon. However, lunar eclipses and shadowing can obscure limb visibility, reducing system reliability. Triangulation techniques necessitate multiple cameras aimed at geometrically diverse celestial sources and are similarly vulnerable to stray light interference. Despite their theoretical viability, these systems often suffer from low navigational accuracy.

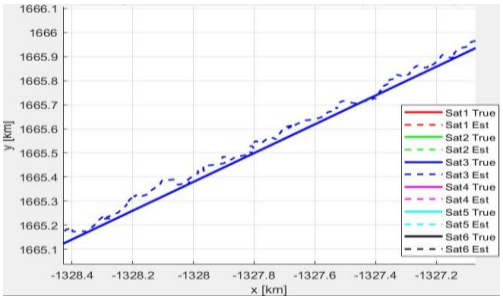

Figure 5: Comparison between true orbits and estimates.

Performance is further affected by variable lighting conditions and the fluctuating number of observable craters across orbital passes. Inter-satellite links, though promising for relative positioning, face limitations in range due to lunar obstruction, and demand precise pointing for optical links.

[1] https:// ssd.jpl.nasa.gov/ tools/ periodic_orbits.html.

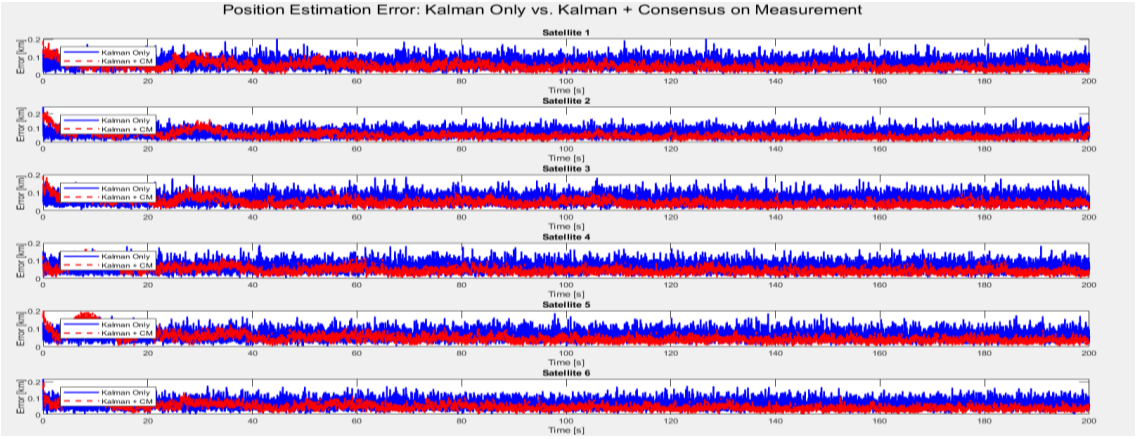

Figure 6: Position error in the 6 satellites using only Kalman filter vs Consensus on Measurement.

The transition from Earth-dependent orbit determination to autonomous navigation in lunar orbit is driven by both operational needs and limitations of current infrastructure. While ground-based tracking networks have enabled positioning accuracies below 40 meters, as demonstrated by missions like KPLO [12], their high operational cost, limited visibility windows, and resource contention make them unsuitable for scalable lunar constellations.

The goal of this work is to enhance the accuracy of state estimation by fusing local sensor measurements through distributed consensus, thereby reducing measurement noise and improving robustness. Each satellite in our constellation implements a local Kalman Filter (KF) to predict and update its state. In its basic form, for each sensor i, the KF algorithm predicts the state at instant k as follows:

$$x_{i,pred} = Ax_{i,est}^{(k-1)} \quad (3)$$

$$P_{i,pred}^{(k)} = AP_{i,est}^{(k-1)}A^T + Q, \quad (4)$$

where $x_{i,pred/est}$ is the state vector predicted or estimated, A is the state transition matrix (based on a constant-velocity model), Q is the process noise covariance. And é is the prediction state. Measurement innovation is computed through

$$\eta_i^{(k)} = z_i^{(k)} - Hx_{i,pred}^{(k)}, \quad (5)$$

where H is the measurement matrix (extracting only the position) and z_i is the sensor measurement. Then, the Kalman gain is computed through

$$K_i^{(k)} = P_{i,pred}^{(k)}H^T\left(HP_{i,pred}^{(k)}H^T + R\right)^{-1}, \quad (6)$$

where R is the measurement noise covariance. Finally, a standard KF update is computed through

$$x_{i,est}^{(k)} = x_{i,pred}^{(k)} + K_i^{(k)}\eta_i^{(k)} \quad (7)$$

$$P_{i_{est}}^{(k)} = P_{i,pred}^{(k)} - K_i^{(k)}HP_{i,pred}^{(k)} \quad (8)$$

as well as the consensus on Measurement update.

Rather than using the individual innovation $\eta^{(k)}$ directly, a consensus process is applied across all sensors to fuse these innovations [13] [14]

$$\eta_{i,CM}^{(k)} = \eta^{(k)} + \epsilon \sum_{j\in N_i}(\eta_j^{(k)} - \eta_i^{(k)}). \quad (9)$$

Once the consensus process converges (i.e. the difference between successive iterations of the innovation is below a set threshold), the fused innovation $\eta_{i,CM}^{(k)}$ is then used in the KF update:

$$x_{i,est}^{(k)} = x_{i,pred}^{(k)} + K_i^{(k)}\eta_{i,CM}^{(k)} \quad (10)$$

For all simulations, the position measurements are assumed to have an error of 100 m in each direction (value is derived from the literature [15]). In our implementation, this is modeled by adding a Gaussian error with a standard deviation of 0.1 km to the true position, as in [16].

In our orbit scenario at 600 km altitude, inter-satellite communication is subject to line-of-sight constraints and limited communication ranges. Consequently, a fully connected network, where each satellite communicates with every other, is often impractical. Instead, a ring network, where each satellite communicates only with its two immediate neighbors, provides a more realistic communication topology. With a CM gain $\epsilon = 0.05$, we compared two approaches, that are shown in Figure 6: i) Pure Kalman Filter: the standard Kalman filter update using only local measurements results in a final position estimation error of approximately 65 m; ii) Kalman Filter with Consensus on Measurements (CM): by fusing the local measurement innovations across the ring network through consensus (with a maximum of 55 iterations per time step), the final position estimation error is reduced to about 46 m a performance improvement of roughly 16%.

These results demonstrate that even in a constrained communication topology such as a ring network, the Consensus on Measurements approach can effectively reduce the measurement noise and enhance state estimation accuracy, thus providing a more robust solution for autonomous navigation in lunar orbit.

IV. Pointing System

The pointing system is a key component of the Moon-orbiting architecture, responsible for power transmission via laser beam. The system, described in detail in [7], is responsible for directing the high-power laser beam to a target with meter-level dimensions, hundreds of kilometers away. This operation must be carried out in a highly noisy environment, particularly in terms of vibration. Therefore, the main challenges associated with pointing are achieving high accuracy and ensuring isolation from micro-vibrations. To address these issues, the system is divided into three stages that are passively and actively isolated from each other: i) Satellite Guidance Navigation and Control (GNC); ii) 2-axis handling system (Figure 11); iii) Fine Steering Mirror [17]); The objective of this study is to numerically evaluate the impact of micro-vibrations, mainly generated by Reaction

Wheels and other mechanical systems on board the satellite [18], on the pointing error of the laser beam toward the receiver.

The assumptions made for this analysis are: i) Circular orbit at 600 km; ii) Transmission Cone angle of 60 ° as explained in [7]; iii) Receiver on the lunar surface with a diameter of 10 meters; iv) Allowable linear error with respect to the receiver center of 1 meter. Based on the above geometric relationships and assumptions, the maximum allowable error is $\theta_{\text{lim}} = 1.5\ \mu\text{rad} = 0.31$ arcsec. The spectrum of micro-vibrations strongly depends on the specific individual characteristics of the satellite; however, as previously mentioned, the contribution of the Reaction Wheels is particularly significant.

Before making detailed assumptions about the other onboard systems, the Power Spectral Density (PSD) model, known as 'ESA model' [19] also shown in Figure 7, based on historical measurements collected from various satellites in orbit over the years, was considered as a baseline. The Power Spectral Density (PSD) is defined as:

$$S(f) = \frac{160}{1+f^2} \tag{11}$$

The root mean square (rms) of the vibrations can be derived from the square root of the PSD. Assuming the micro-vibrations follow a Gaussian distribution with zero mean, the requirement that 3 σ remains below the previously calculated θ_{lim} can be formulated. This leads to the identification of a maximum relevant frequency of 27 Hz. According to the literature, the GNC system is capable of operating down to 1 Hz. The pointing system is therefore responsible for compensating for disturbances in the frequency range between 1 and 27 Hz, as can be seen in Figure 8.

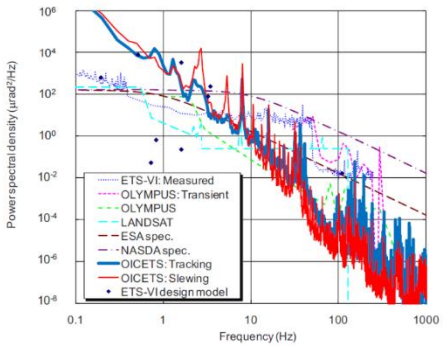

Figure 7: Real measurements of micro-vibrations induced at different satellites, compared with ESA specification. [19]

To include micro-vibrations in the Simulink model, a signal having the ESA PSD was generated for each axis using the following procedure: i) White noise generation with mean 0 and unit variance, corresponding to “flat” PSD; ii) Fast Fourier Transform (FFT) of the generated signal calculation; iii) Multiplication of the amplitude of each bin of the FFT by $\sqrt{S(f)}$; iv) Inverse Fast Fourier Transform (IFFT) calculation. The results are shown in Figure 9.

For verification purposes, a 60-second simulation is carried out, in which angular micro-vibrations are applied on each axis using three signals generated with the described procedure. The logarithmic heat map of the reflected beam position at the receiver, representative of the pointing error attributable to the micro-vibrations, is reported in Figure 10.

The generated signals have a maximum amplitude of around 80 μrad, which is consistent with the maximum linear error of 50 m obtained from the simulation.

This result was obtained by considering satellite and pointing mechanism as perfectly rigid.

The inverse kinematic analysis of the mechanism, considering only the variation of angle θ_{alt} shows that:

To compensate for micro-vibrations (maximum angle 50 μrad), an extension between $\pm 8\ \mu m$ is required compared to the rest configuration ($\theta_{alt} = \theta_{az} = 0$).

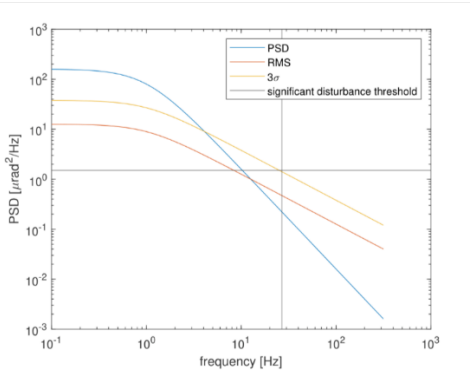

Figure 8: Frequency Disturbance Threshold.

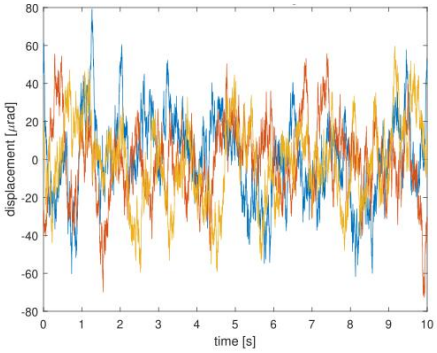

Figure 9: Generated vibration signal.

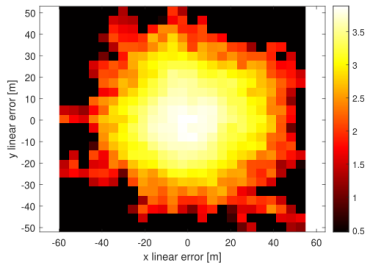

Figure 10: Logarithmic heat map of pointing error.

To compensate for the residual attitude error (assumed to be 1 degree), an extension between $\pm 850\ \mu m$ is required compared to the rest configuration. Therefore, it is estimated that a suitable actuator should have a range of about 2 mm, with an accuracy of 0.15 μm (from θ_{lim}), and a band equal to the maximum significant frequency of 27 Hz previously identified. The accuracy and decoupling described above can

be achieved through the integrated use of three key systems: i) the satellite's GNC, which is responsible for rotating the entire spacecraft during transmission toward the receiver on the surface, with an accuracy of approximately 1°; ii) the 2-axis motion platform which is responsible for passively isolating from the micro- vibrations induced by the satellite bus; and actively directing the FSM; iii) The FSM, the last stage, which precisely adjusts the mirror position via piezoelectric actuators.
Future work involves the integrated simulation of all these three systems currently designed and simulated individually.

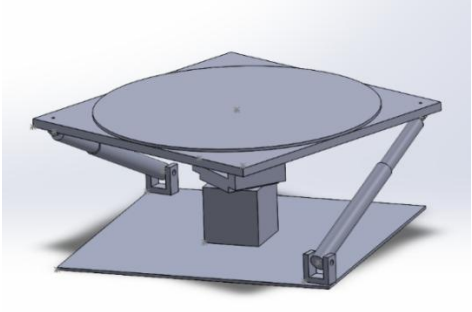

Figure 11: Side view of the 2-axis handling system.

V. ACKNOWLEDGMENT

The authors thanks ASI for funding the research within the call 'Sviluppo di progetti/esperimenti scientifici per la Luna – Development of project/scientific experiments for the Moon.

VI. BIBLIOGRAPHY

[1] J. Csank, "NASA Lunar Surface Operations & Power Grid, Electrical Engineer Power Management and Distribution Branch," NASA Glenn Research Center, 2023.

[2] L. Maskal, C. Singleton, A. Aboudiwan, A. Taha and M. Marciniak, "Solar panels for the lunar base," in *SPIE OPTO*, San Francisco, 2020.

[3] A. K. Ross, S. Ruppert, P. Glaser and M. Elvis, "Preliminary quantification of the available solar power near the lunar South Pole," *Acta Astronautica*, pp. 616-630, 2023.

[4] Y. Ma, L. Jiahao and L. Yue, "Feasibility and Safety Analysis of Solid-State Reactor for Lunar Surface Exploration," in *31st International Conference on Nuclear Engineering*, 2024.

[5] K. Jin and W. Zhou, "Wireless Laser Power Transmission: A Review of Recent Progress," *IEEE Transactions on Power Electronics*, vol. 34, pp. 3842-3859, 2019.

[6] D. Sfasciamuro, A. Mauro, F. Lopez, A. Villa, G. Monteleone and S. Mauro, "A Lunar-Orbiting Satellite Constellation for Wireless Energy Supply," *MDPI*, 2023.

[7] S. Domenico, A. Mauro, A. Villa, F. Lopez and S. Mauro, "Wireless Power Transmission: A New Frontier for Lunar Colonisation Development," in *IEEE Metrology for Aerospace*, 2024.

[8] W. A. Yu, A. M. Krainak, A. M. Stephen, R. J. Chen, B. Coyle, K. Numata, J. Camp, B. J. Abshire, R. G. Allan, X. S. Li and R. Haris, "Fiber Lasers and Amplifiers for Space-based Science and Exploration," Greenbelt, 2012.

[9] N. Platonov, R. Yagodkin, J. De La Cruz, C. Arambula, J. Fitts and V. Sergeev, "7kW single-mode ytterbium fiber laser with beam quality parameter M2<1.1 and direct diode pumping," in *SPIE 13342, Fiber Lasers XXII: Technology and Systems, 1334202*, San Francisco, California, 2025.

[10] M. Lara, "Design of long-lifetime lunar orbits: A hybrid approach," *Acta Astronautica*, vol. 69, no. 3-4, pp. 186-199, 2011.

[11] M. Ovchinnikov, S. Maksim and T. Sergey, "Lunar Satellite Constellations in Frozen Low Orbits," *MDPI Aerospace*, vol. 11, no. 11, p. 918, 2024.

[12] K. Young-Rok, S. Young-Joo, P. Jae-Ik, L. Donghun, B. Jonghee, H. Seungbum and K. Dae-Kwan, "Ground Tracking Support Condition Effect on Orbit Determination for Korea Pathfinder Lunar Orbiter (KPLO) in Lunar Orbit," *Journal of Astronomy and Space Science*, 2020.

[13] L. Wangyan, W. Zidong, W. Guoliang, M. Lifeng, H. Jun and D. Derui, "A Survey on Multisensor Fusion and Consensus Filtering for Sensor Networks," *Discrete Dynamics in Nature and Society*, 2015.

[14] H. Gui and A. H. De Ruiter, "Global Finite-Time Attitude Consensus of Leader-Following Spacecraft Systems Based on Distributed Observers," *Automatica*, 2018.

[15] J. C.-M. X. W. Joshua, K. Yosuke and N. Shinichi, "Autonomous and Earth-Independent Orbit Determination for a Lunar Navigation Satellite System," *Aerospace* , 2024.

[16] K. Liyama, Y. Kawabata and R. Funase, "Autonomous and Decentralized Orbit Determination and Clock Offset Estimation of Lunar Navigation Satellites Using GPS Signals and Inter-Satellite Ranging," in *34th International Technical Meeting of the Satellite Division of The Institute of Navigation (ION GNSS+ 2021)*, 2021.

[17] M. Ostaszewski and W. Vermeer, "Fine steering mirror for the James Webb Space Telescope - art. no. 66650D," in *The International Society for Optical Engineering*, 2007.

[18] S. Raffa, *Master Thesis: Spacecraft Micro-vibrations Analysis for Optical Communication Payloads*, Torino: Politecnico di Torino, 2020.

[19] M. E. Wittig, L. Van Holtz, D. Tunbridge and H. C. Vermeulen, "In-orbit measurements of microaccelerations of ESA's communication satellite Olympus," *Free-Space Laser Communication Technologies*, 1990.